

Scalable intensity-based photonic matrix-vector multiplication processor using single-wavelength time-division-multiplexed signals

CHENGLI CHAI,¹ RUI TANG,^{1,*} MAKOTO OKANO,² KASIDIT TOPRASERTPONG,¹ SHINICHI TAKAGI,¹ AND MITSURU TAKENAKA¹

¹Department of Electrical Engineering and Information Systems, The University of Tokyo, Tokyo 113-8656, Japan

²National Institute of Advanced Industrial Science and Technology, Ibaraki 305-8568, Japan

*ruitang@mosfet.t.u-tokyo.ac.jp

Received XX Month XXXX; revised XX Month, XXXX; accepted XX Month XXXX; posted XX Month XXXX (Doc. ID XXXXX); published XX Month XXXX

Photonic integrated circuits provide a compact platform for ultrafast and energy-efficient matrix-vector multiplications (MVMs) in the optical domain. Recently, schemes based on time-division multiplexing (TDM) have been proposed as scalable approaches for realizing large-scale photonic MVM processors. However, existing demonstrations rely on coherent detection or multiple wavelengths, both of which complicate their operations. In this work, we demonstrate a scalable TDM-based photonic MVM processor that uses only single-wavelength intensity-modulated optical signals, thereby avoiding coherent detection and enabling simplified operations. A 32-channel processor is fabricated on a Si-on-insulator (SOI) platform and used to experimentally perform convolution operations in a convolutional neural network (CNN) for handwritten digit recognition, achieving a classification accuracy of 93.47% for 1500 images.

Introduction. The growing size of deep learning models has made power consumption a critical challenge, with matrix multiplications identified as a major performance bottleneck. While graphics processing units (GPUs) are widely used to

accelerate these computations, improvements in energy efficiency have slowed as Moore’s law approaches its limit. This has driven the development of energy-efficient hardware accelerators for deep learning. Photonic neural networks (PNNs) have emerged as a promising solution, enabling analog matrix-vector multiplications (MVMs) on compact photonic integrated circuits with exceptional speed and energy efficiency [1–4]. Various architectures for photonic MVM have been proposed, including coherent architectures that use both the amplitude and phase information of light [5–8], and intensity-based architectures that use only the amplitude information [9–14]. However, the scalability of these architectures is rather limited due to the need for a large number of optical modulators—typically N^2 optical modulators are required to represent an $N \times N$ matrix. Recently, scalable architectures based on time-division multiplexing (TDM) have been proposed [15–21], in which the number of optical modulators is significantly reduced from N^2 to N for the same matrix size. Despite this progress, the operations of existing TDM-based devices are still relatively complicated due to the need for coherent detection or multiple wavelengths [16,17,21], and large-scale demonstrations are still lacking.

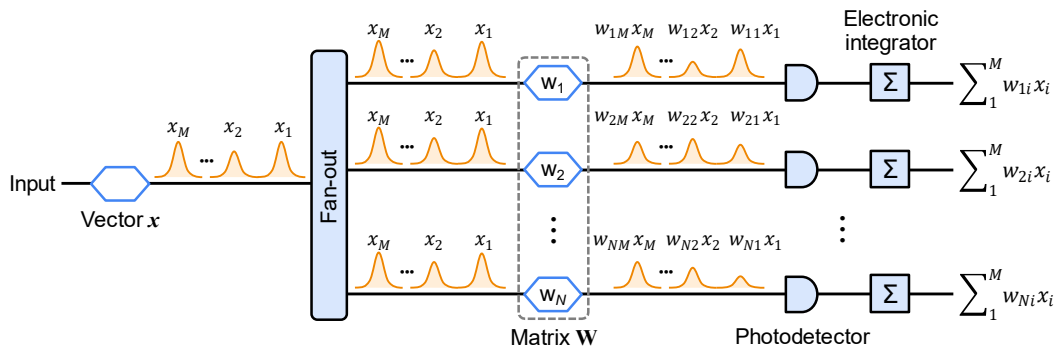


Fig. 1. Operation principle of this scheme. A single-wavelength input light is modulated by an optical intensity modulator, which generates an M -element vector x by sequentially encoding each element onto the light intensity. These TDM signals are equally split into N channels and further modulated by N modulators, each generating one row in an $N \times M$ matrix \mathbf{W} . The two intensity modulations perform the multiplication between the vector and matrix elements. These signals are detected by photodetectors, generating photocurrents proportional to the optical power, which are then integrated by electronic integrators to perform the accumulation operation.

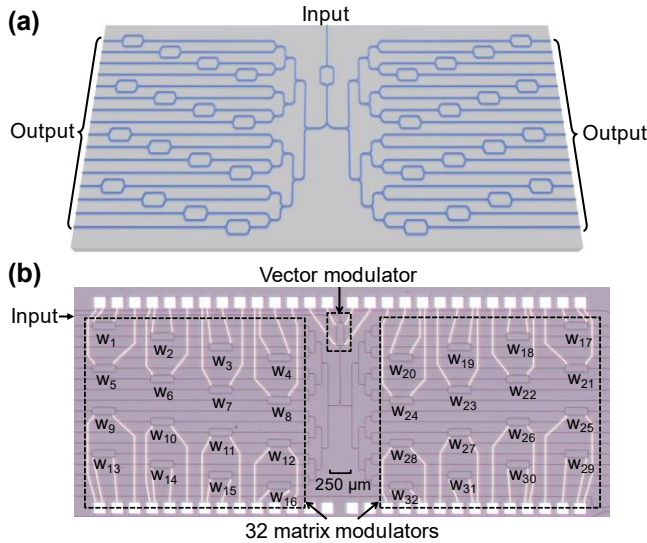


Fig. 2. (a) Schematic structure of the 32-channel processor. (b) A microscope image of the 32-channel processor fabricated on an SOI platform.

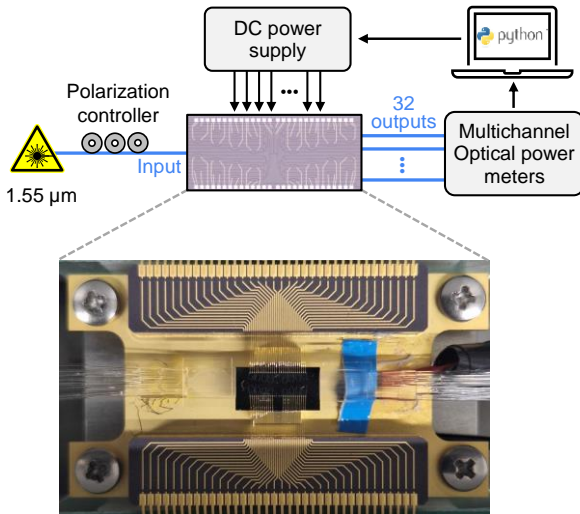


Fig. 3. Experimental setup and an image of the packaged chip. The chip is wire-bonded for electrical connections and packaged with two fiber arrays.

In this work, we propose and demonstrate a scalable TDM-based photonic MVM processor that uses only single-wavelength intensity-modulated optical signals, thereby avoiding coherent detection and enabling simplified operations. A large-scale ($N=32$) processor is fabricated on a Si-on-insulator (SOI) platform and used to perform convolution operations in a convolutional neural network (CNN) for handwritten digit recognition, achieving a classification accuracy of 93.47%.

Results. The operation principle of this scheme is illustrated in Fig. 1. A single-wavelength input light is modulated by an optical intensity modulator, which generates an M -element vector \mathbf{x} by sequentially encoding each element onto the light intensity. Note that M can be arbitrary. These TDM signals are equally split into N channels and further modulated by N

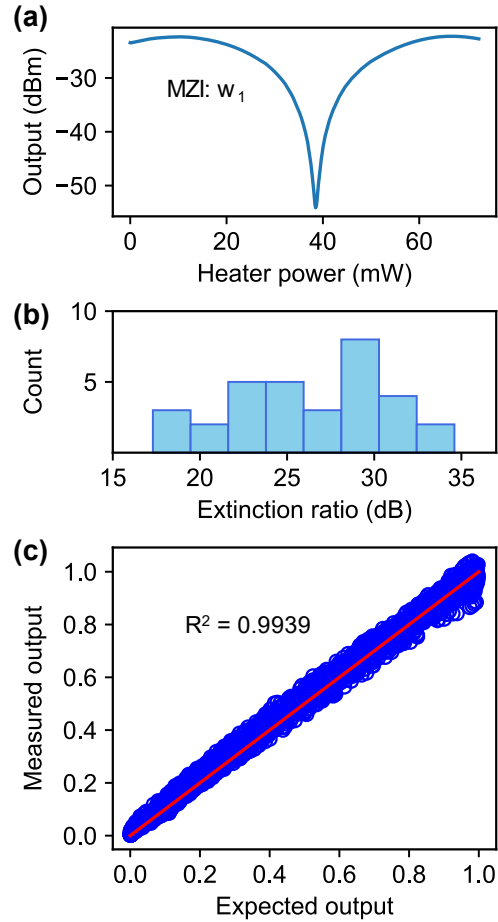


Fig. 4. (a) Characterization result of one MZI (w_1) when sweeping the electric power applied to the thermo-optic phase shifter, exhibiting an extinction ratio of 31.9 dB. (b) Measured extinction ratios for all 32 matrix MZIs. (c) Normalized measured output powers and expected output powers when 100 sets of random configurations are applied to all MZIs. A total of 3200 points are plotted, showing a high determination coefficient (R^2) of 0.9939.

modulators, each generating one row in an $N \times M$ matrix \mathbf{W} . The two intensity modulations perform the multiplication between the vector and matrix elements. These signals are detected by photodetectors, generating photocurrents proportional to the optical power, which are then integrated by electronic integrators to perform the accumulation operation [15]. Here, high-speed intensity modulators are desired, and the vector and matrix modulators should be synchronized to function properly.

To demonstrate this concept, a 32-channel ($N=32$) processor is fabricated on an SOI platform by a commercial foundry (Applied Nanotools) using electron-beam lithography. The schematic structure and a microscope image of the processor are shown in Fig. 2. The Si waveguides have a standard core size of $500 \times 220 \text{ nm}^2$ and a typical propagation loss of 1.2 dB/cm. Edge couplers based on inverse tapers are used to couple light into and out of the chip. Cascaded stages of 1×2 multimode interference (MMI) couplers are used to split the light into 32 channels. Tunable Mach-Zehnder interferometers (MZIs) are employed as intensity modulators,

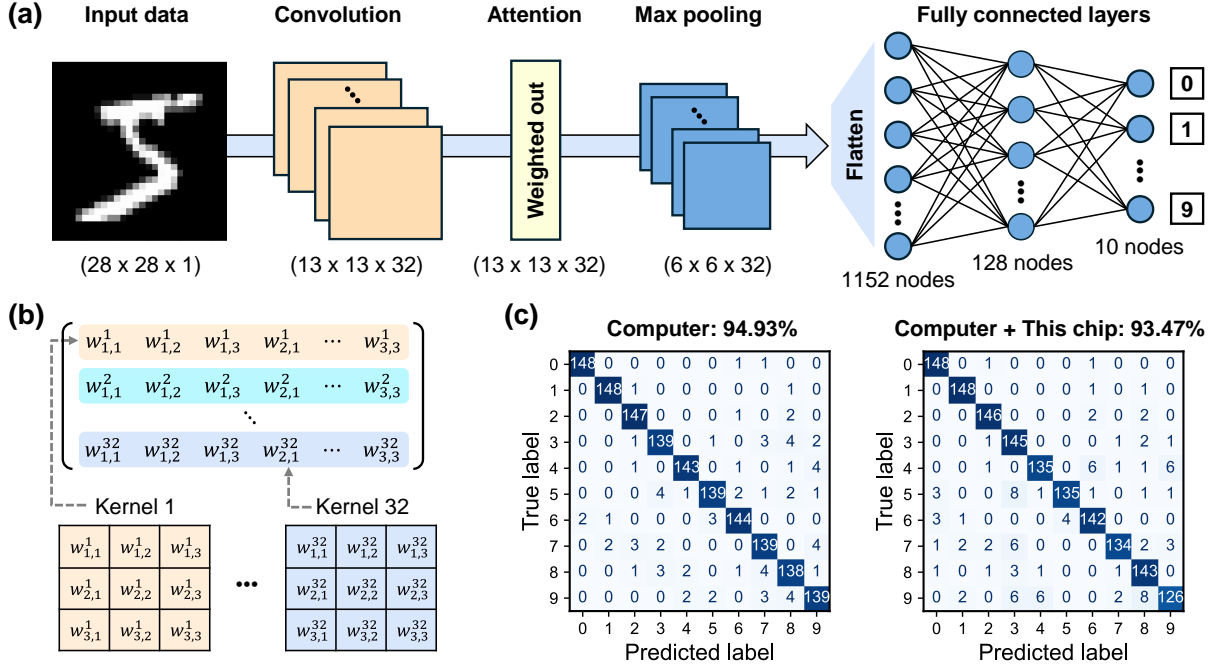


Fig. 5. (a) A CNN constructed for handwritten digit recognition, which consists of a convolution layer, an attention layer, a max pooling layer, and fully connected layers. (b) Converting 32 kernels into a 32×9 matrix for implementation on the photonic processor. Each 3×3 kernel is flattened into a row in the matrix. (c) Classification results for 1500 MNIST images when the inference is performed using a computer alone (left) and when the 32-channel processor is used to perform the convolution operations (right).

using thermo-optic phase shifters (length: 220 μm, width: 4 μm) with a power consumption of less than 30 mW/π. Since the operation speed of thermo-optic phase shifters is not sufficiently fast, they are used here only for proof-of-concept purposes. High-speed electro-optic modulators or electro-absorption modulators should be employed in practical scenarios [8,22,23]. While photodetectors are not integrated on this chip due to platform limitations, they can be easily integrated onto the same chip using other foundry services [24]. The electronic integrator can be implemented following the method described in [16]. The chip is wire-bonded for electrical connections and packaged with two fiber arrays, with coupling losses ranging from 2.7 to 4.5 dB per coupling. Figure 3 shows the experimental setup and the packaged chip. Continuous-wave light at a wavelength of 1.55 μm is injected into the chip after its polarization is adjusted to transverse electric (TE). The chip temperature is stabilized at room temperature using a thermoelectric cooler. All phase shifters on the chip are driven by a 40-channel direct current (DC) power supply (NicsLab, XDAC-40MUB-R4G8). Light signals from the 32 output ports are detected by two multi-channel optical power meters (Santec, OP760).

Each MZI is characterized to create a lookup table that maps the electric power applied to the phase shifter to the normalized MZI transmittance. The result for one MZI is shown in Fig. 4(a), exhibiting an extinction ratio of 31.9 dB. The measured extinction ratios of all matrix MZIs are plotted in Fig. 4(b), with a mean value of 26.1 dB. Random initial phases are observed among the MZIs due to fabrication imperfections. After creating lookup tables for all MZIs, we applied 100 sets of random configurations to all MZIs and

measured output powers at all output ports. The measured powers were normalized and compared with the expected values, as shown in Fig. 4(c), which contains 3200 points in total. The determination coefficient (R^2) is as high as 0.9939, indicating the high operation fidelity of the fabricated chip.

A CNN for handwritten digit recognition is constructed, as shown in Fig. 5(a). This CNN consists of a convolution layer, an attention layer, a max pooling layer, and fully connected layer. It is trained on the MNIST dataset, which contains 60000 training images and 10000 test images. Each image is a single-channel grayscale image with 28×28 pixels. The convolution layer uses 32 kernels (kernel size: 3×3, stride: 2, padding: 0), which convert an input image into 13×13×32 feature maps. All kernel elements are constrained between 0 and 1 during training to enable implementation on the photonic processor. These feature maps then pass through a simple attention layer [25], which computes attention scores and generates a weighted output. The attention scores are stored in a 13×13 matrix \mathbf{S} , calculated as

$$\mathbf{S} = \text{Softmax}(\mathbf{I}_{13 \times 13 \times 32} \mathbf{A}_{32 \times 1}), \quad (1)$$

where $\mathbf{I}_{13 \times 13 \times 32}$ represents the input feature maps, $\mathbf{A}_{32 \times 1}$ represents a trainable weight vector, and Softmax represents the softmax function. $\mathbf{A}_{32 \times 1}$ is optimized automatically during training. The weighted output is then generated as

$$\mathbf{O} = \mathbf{I}_{13 \times 13 \times 32} \odot \mathbf{S}_{13 \times 13}, \quad (2)$$

where \odot represents the Hadamard product. The output is next processed through a max pooling layer (pool size: 2×2) and flattened into a vector, which is then processed by fully connected layers. Dropout layers are applied after the pooling layer and the first fully connected layer during training, with dropout probabilities of 0.25 and 0.5, respectively. The

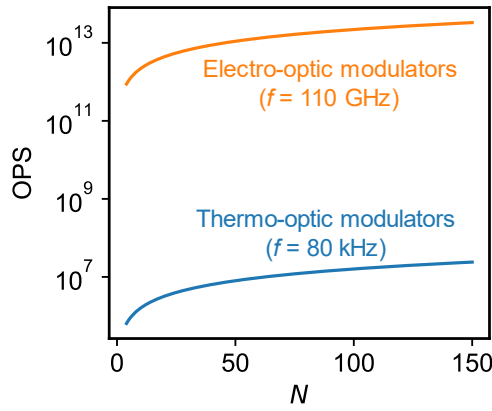


Fig. 6. Estimated computation speeds for this scheme under varying modulator types and matrix scales.

dropout layers are deactivated during inference. The rectified linear unit (ReLU) and softmax function are used as the nonlinear activators for the first and second fully connected layers, respectively. This CNN is trained on a computer using the Adam optimizer and the categorical cross-entropy loss function.

The 32-channel processor is used to perform the convolution operations by converting the 32 kernels into a 32×9 matrix, as illustrated in Fig. 5(b). Each 3×3 kernel is flattened into a row in the matrix, and each convolution region in the input image is flattened into a 9×1 vector. Thus, the convolution operations are executed as the multiplication of a 32×9 matrix and 9×1 vectors. For simplicity, the accumulation operation is performed on a computer by directly summing the measured outputs. The classification results for 1500 images are shown in Fig. 5(c). When using the computer alone, the classification accuracy is 94.93%. By performing the convolution operations on the photonic chip, a classification accuracy of 93.47% is experimentally achieved, further demonstrating the high operation fidelity of this chip.

The computation speed in operations per second (OPS) for this scheme is given by

$$\text{OPS} = 2fN, \quad (3)$$

where f is the clock frequency, and the factor of 2 accounts for simultaneous multiplication and accumulation operations within one modulation cycle. For this chip, assuming f is 80 kHz, which corresponds to a switching time of $12.5 \mu\text{s}$ [26], the computation speed is 5.12×10^6 OPS. The estimated computation speeds at various clock frequencies and matrix scales are shown in Fig. 6. Compact intensity modulators with 3-dB bandwidths exceeding 110 GHz have been demonstrated on both SOI and thin-film lithium niobate (TFLN) platforms [27,28]. If such modulators are used, a high computation speed of 2.82×10^{13} OPS can be achieved with $N=128$.

Conclusion. We have demonstrated a scalable, intensity-based photonic MVM processor using single-wavelength TDM signals. A 32-channel processor was fabricated on an SOI platform and used to perform convolution operations in a CNN for handwritten digit recognition, achieving a

classification accuracy of 93.47% for 1500 images. By further replacing thermo-optic modulators with high-speed electro-optic modulators, high-speed and energy-efficient MVMs can be performed using this architecture.

Funding. Japan Science and Technology Agency (CREST, JPMJCR2004); Japan Society for the Promotion of Science (22K14298).

Disclosures. The authors are aware of a recent preprint that demonstrates a similar architecture on a thin-film lithium niobate platform [23].

Data availability. Data underlying the results presented in this paper are available from the corresponding author upon reasonable request.

References

1. Y. Shen, N. C. Harris, S. Skirlo, *et al.*, Nat. Photonics **11**, 441 (2017).
2. B. J. Shastri, A. N. Tait, T. Ferreira de Lima, *et al.*, Nat. Photonics **15**, 102 (2021).
3. H. Zhou, J. Dong, J. Cheng, *et al.*, Light Sci. Appl. **11**, 30 (2022).
4. Z. Xu, T. Zhou, M. Ma, *et al.*, Science **384**, 202 (2024).
5. W. R. Clements, P. C. Humphreys, B. J. Metcalf, *et al.*, Optica **3**, 1460 (2016).
6. R. Tang, R. Tanomura, T. Tanemura, *et al.*, ACS Photonics **8**, 2074 (2021).
7. G. Giamougiannis, A. Tsakyridis, Y. Ma, *et al.*, J. Light. Technol. **41**, 2425 (2023).
8. M. Moralis-Pegios, G. Giamougiannis, A. Tsakyridis, *et al.*, Nat. Commun. **15**, 5468 (2024).
9. A. N. Tait, T. F. de Lima, E. Zhou, *et al.*, Sci. Rep. **7**, 7430 (2017).
10. J. Feldmann, N. Youngblood, M. Karpov, *et al.*, Nature **589**, 52 (2021).
11. R. Yin, H. Xiao, Y. Jiang, *et al.*, Optica **10**, 1709 (2023).
12. R. Tang, S. Ohno, K. Tanizawa, *et al.*, Photonics Res. **12**, 1681 (2024).
13. R. Tang, M. Okano, C. Zhang, *et al.*, arXiv:2410.05956 (2014).
14. T. Xu, W. Zhang, J. Zhang, *et al.*, Optica **11**, 1039 (2024).
15. R. Hamerly, L. Bernstein, A. Sludds, *et al.*, Phys. Rev. X **9**, 021032 (2019).
16. A. Sludds, S. Bandyopadhyay, Z. Chen, *et al.*, Science **378**, 270 (2022).
17. S. Rahimi Kari, N. A. Nobile, D. Pantin, *et al.*, Optica **11**, 542 (2024).
18. R. Hamerly, A. Sludds, S. Bandyopadhyay, *et al.*, J. Light. Technol. **42**, 7795 (2024).
19. C. Pappas, T. Moschos, M. Moralis-Pegios, *et al.*, in *Optical Fiber Communication Conference (OFC) 2024*, paper Th3G.1.
20. C. Pappas, T. Moschos, A. Prapas, *et al.*, in *Optical Fiber Communication Conference (OFC) 2024*, paper Th4C.3.
21. S. Ou, K. Xue, L. Zhou, *et al.*, arXiv:2401.18050 (2024).
22. Z. Lin, B. J. Shastri, S. Yu, *et al.*, Nat. Commun. **15**, 9081 (2024).
23. Y. Hu, Y. Song, X. Zhu, *et al.*, arXiv:2411.02734 (2024).
24. S. Y. Siew, B. Li, F. Gao, *et al.*, J. Light. Technol. **39**, 4374 (2021).
25. J. Park, S. Woo, J.-Y. Lee, *et al.*, Int. J. Comput. Vis. **128**, 783 (2020).
26. R. B. Priti, G. Zhang, and O. Liboiron-Ladouceur, Opt. Express **27**, 14199 (2019).
27. C. Han, Z. Zheng, H. Shu, *et al.*, Sci. Adv. **9**, eadi5339 (2023).
28. B.-C. Pan, H.-X. Liu, H.-C. Xu, *et al.*, Chip **1**, 100029 (2022).

References

1. Y. Shen, N. C. Harris, S. Skirlo, M. Prabhu, T. Baehr-Jones, M. Hochberg, X. Sun, S. Zhao, H. Larochelle, D. Englund, and M. Soljačić, "Deep learning with coherent nanophotonic circuits," *Nat. Photonics* **11**, 441–446 (2017).
2. B. J. Shastri, A. N. Tait, T. Ferreira de Lima, W. H. P. Pernice, H. Bhaskaran, C. D. Wright, and P. R. Prucnal, "Photonics for artificial intelligence and neuromorphic computing," *Nat. Photonics* **15**, 102–114 (2021).
3. H. Zhou, J. Dong, J. Cheng, W. Dong, C. Huang, Y. Shen, Q. Zhang, M. Gu, C. Qian, H. Chen, Z. Ruan, and X. Zhang, "Photonic matrix multiplication lights up photonic accelerator and beyond," *Light Sci. Appl.* **11**, 30 (2022).
4. Z. Xu, T. Zhou, M. Ma, C. Deng, Q. Dai, and L. Fang, "Large-scale photonic chiplet Taichi empowers 160-TOPS/W artificial general intelligence," *Science* **384**, 202–209 (2024).
5. W. R. Clements, P. C. Humphreys, B. J. Metcalf, W. S. Kolthammer, and I. A. Walsmley, "Optimal design for universal multiport interferometers," *Optica* **3**, 1460–1465 (2016).
6. R. Tang, R. Tanomura, T. Tanemura, and Y. Nakano, "Ten-port unitary optical processor on a silicon photonic chip," *ACS Photonics* **8**, 2074–2080 (2021).
7. G. Giamougiannis, A. Tsakyridis, Y. Ma, A. Totović, M. Moralis-Pegios, D. Lazovsky, and N. Pleros, "A Coherent Photonic Crossbar for Scalable Universal Linear Optics," *J. Light. Technol.* **41**, 2425–2442 (2023).
8. M. Moralis-Pegios, G. Giamougiannis, A. Tsakyridis, D. Lazovsky, and N. Pleros, "Perfect linear optics using silicon photonics," *Nat. Commun.* **15**, 5468 (2024).
9. A. N. Tait, T. F. de Lima, E. Zhou, A. X. Wu, M. A. Nahmias, B. J. Shastri, and P. R. Prucnal, "Neuromorphic photonic networks using silicon photonic weight banks," *Sci. Rep.* **7**, 7430 (2017).
10. J. Feldmann, N. Youngblood, M. Karpov, H. Gehring, X. Li, M. Stappers, M. Le Gallo, X. Fu, A. Lukashchuk, A. S. Raja, J. Liu, C. D. Wright, A. Sebastian, T. J. Kippenberg, W. H. P. Pernice, and H. Bhaskaran, "Parallel convolutional processing using an integrated photonic tensor core," *Nature* **589**, 52–58 (2021).
11. R. Yin, H. Xiao, Y. Jiang, X. Han, P. Zhang, L. Chen, X. Zhou, M. Yuan, G. Ren, A. Mitchell, and Y. Tian, "Integrated WDM-compatible optical mode division multiplexing neural network accelerator," *Optica* **10**, 1709–1718 (2023).
12. R. Tang, S. Ohno, K. Tanizawa, K. Ikeda, M. Okano, K. Toprasertpong, S. Takagi, and M. Takenaka, "Symmetric silicon microring resonator optical crossbar array for accelerated inference and training in deep learning," *Photonics Res.* **12**, 1681–1688 (2024).
13. R. Tang, M. Okano, C. Zhang, K. Toprasertpong, S. Takagi, and M. Takenaka, "Waveguide-multiplexed photonic matrix-vector multiplication processor using multiport photodetectors," *arXiv:2410.05956* (2024).
14. T. Xu, W. Zhang, J. Zhang, Z. Luo, Q. Xiao, B. Wang, M. Luo, X. Xu, B. J. Shastri, P. R. Prucnal, and C. Huang, "Control-free and efficient integrated photonic neural networks via hardware-aware training and pruning," *Optica* **11**, 1039–1049 (2024).
15. R. Hamerly, L. Bernstein, A. Sludds, M. Soljačić, and D. Englund, "Large-scale optical neural networks based on photoelectric multiplication," *Phys. Rev. X* **9**, 021032 (2019).
16. A. Sludds, S. Bandyopadhyay, Z. Chen, Z. Zhong, J. Cochrane, L. Bernstein, D. Bunandar, P. B. Dixon, S. A. Hamilton, M. Streshinsky, A. Novack, T. Baehr-Jones, M. Hochberg, M. Ghobadi, R. Hamerly, and D. Englund, "Delocalized photonic deep learning on the internet's edge," *Science* **378**, 270–276 (2022).
17. S. Rahimi Kari, N. A. Nobile, D. Pantin, V. Shah, and N. Youngblood, "Realization of an integrated coherent photonic platform for scalable matrix operations," *Optica* **11**, 542–551 (2024).
18. R. Hamerly, A. Sludds, S. Bandyopadhyay, Z. Chen, Z. Zhong, L. Bernstein, and D. Englund, "Netcast: low-power edge computing with WDM-defined optical neural networks," *J. Light. Technol.* **42**, 7795–7806 (2024).
19. C. Pappas, T. Moschos, M. Moralis-Pegios, G. Giamougiannis, A. Tsakyridis, M. Kirtas, N. Passalis, A. Tefas, and N. Pleros, "A teraFLOP photonic matrix multiplier using time-space-wavelength multiplexed AWGR-based architectures," in *Optical Fiber Communication Conference (OFC) 2024* (Optica Publishing Group, 2024), paper Th3G.1.
20. C. Pappas, T. Moschos, A. Prapas, A. Tsakyridis, M. Moralis-Pegios, K. Vyrsoinos, and N. Pleros, "A 160 TOPS multi-dimensional AWGR-based accelerator for deep learning," in *Optical Fiber Communication Conference (OFC) 2024* (Optica Publishing Group, 2024), paper Th4C.3.
21. S. Ou, K. Xue, L. Zhou, C. Lee, A. Sludds, R. Hamerly, K. Zhang, H. Feng, R. Koppurapu, E. Zhong, C. Wang, D. Englund, M. Yu, and Z. Chen, "Hypermultiplexed integrated-photonics-based tensor optical processor," *arXiv:2401.18050* (2024).
22. Z. Lin, B. J. Shastri, S. Yu, J. Song, Y. Zhu, A. Safarnejadian, W. Cai, Y. Lin, W. Ke, M. Hammood, T. Wang, M. Xu, Z. Zheng, M. Al-Qadasi, O. Esmaeli, M. Rahim, G. Pakulski, J. Schmid, P. Barrios, W. Jiang, H. Morison, M. Mitchell, X. Guan, N. A. F. Jaeger, L. A. Rusch, S. Shekhar, W. Shi, S. Yu, X. Cai, and L. Chrostowski, "120 GOPS photonic tensor core in thin-film lithium niobate for inference and in situ training," *Nat. Commun.* **15**, 9081 (2024).
23. Y. Hu, Y. Song, X. Zhu, X. Guo, S. Lu, Q. Zhang, L. He, C. A. A. Franken, K. Powell, H. Warner, D. Assumpcao, D. Renaud, Y. Wang, L. Magalhães, V. Rosborough, A. Shams-Ansari, X. Li, R. Cheng, K. Luke, K. Yang, G. Barbastathis, M. Zhang, D. Zhu, L. Johansson, A. Beling, N. Sinclair, and M. Loncar, "Integrated lithium niobate photonic computing circuit based on efficient and high-speed electro-optic conversion," *arXiv:2411.02734* (2024).
24. S. Y. Siew, B. Li, F. Gao, H. Y. Zheng, W. Zhang, P. Guo, S. W. Xie, A. Song, B. Dong, L. W. Luo, C. Li, X. Luo, and G.-Q. Lo, "Review of silicon photonics technology and platform development," *J. Light. Technol.* **39**, 4374–4389 (2021).
25. J. Park, S. Woo, J.-Y. Lee, and I. S. Kweon, "A simple and lightweight attention module for convolutional neural networks," *Int. J. Comput. Vis.* **128**, 783–798 (2020).
26. R. B. Priti, G. Zhang, and O. Liboiron-Ladouceur, "3×10 Gb/s silicon three-mode switch with 120° hybrid based unbalanced Mach-Zehnder interferometer," *Opt. Express* **27**, 14199–14212 (2019).
27. C. Han, Z. Zheng, H. Shu, M. Jin, J. Qin, R. Chen, Y. Tao, B. Shen, B. Bai, F. Yang, Y. Wang, H. Wang, F. Wang, Z. Zhang, S. Yu, C. Peng, and X. Wang, "Slow-light silicon modulator with 110-GHz bandwidth," *Sci. Adv.* **9**, eadi5339 (2023).
28. B.-C. Pan, H.-X. Liu, H.-C. Xu, Y.-S. Huang, H. Li, Z.-J. Yu, L. Liu, Y.-C. Shi, and D.-X. Dai, "Ultra-compact lithium niobate microcavity electro-optic modulator beyond 110 GHz," *Chip* **1**, 100029 (2022).